2015

Differential diffusion and salt finger fluxes in a stratified turbulent laboratory system

Ian Paul Willard
Iowa State University

Differential diffusion and salt finger fluxes in a stratified turbulent laboratory system

by

Ian Paul Willard

A thesis submitted to the graduate faculty

in partial fulfillment of the requirements for the degree of

MASTER OF SCIENCE

Major: Civil Engineering (Environmental Engineering)

Program of Study Committee:
Chris Rehmann, Major Professor
Roy Gu
William Simpkins

Iowa State University

Ames, Iowa

2015

TABLE OF CONTENTS

LIST OF FIGURES

ACKNOWLEDGMENTS

I would like to express my gratitude to Iowa State University and the National Science Foundation (grant number 1034221) for the opportunity and funding to work on such an interesting project. I want to thank Dr. Chris Rehmann for serving as my advisor. I learned a lot by working under him, and I enjoyed our frequent conversations about both technical and other topics. I am also grateful to Dr. William Simpkins and Dr. Roy Gu for serving on my committee and offering valuable feedback. I want to thank Dr. Ryan Jackson for allowing me to use his figures, answering occasional questions, and keeping meticulous notes when he ran his experiments. I want to thank the members of my research group, Cindy Maroney, Zhimin Li, Rusen Sinir, and Lauren Schwab, for listening to me discuss my research and for offering input. I enjoyed working with each one of them. Finally, I am grateful to my family and friends for supporting me over the past two years. I am thankful that I had people to encourage me, and occasionally distract me, throughout the process.

ABSTRACT

A series of laboratory experiments was run with a variety of stable temperature profiles, unstable salinity profiles, and stable density profiles. The fluid was periodically stirred at set turbulence intensities and profiled after each stirring period. Salt fingers and differential diffusion were both present during stable temperature and unstable salinity conditions with turbulence. When the density ratio R_ρ was between 1 and approximately 3, salt finger fluxes were dominant and caused the salinity to mix faster than the temperature. When R_ρ was greater than about 4, differential diffusion fluxes were dominant and caused temperature to mix faster than salinity. The differential diffusion and salt finger fluxes were also dependent on the turbulence intensity. Differential diffusion fluxes were stronger for large values of the turbulent Richardson number Ri_T than for small values of Ri_T. However, salt finger fluxes were stronger for small values of Ri_T than for large values of Ri_T. During periods of turbulence, the mixing efficiencies were generally highest in the regions that were most conducive to differential diffusion.

CHAPTER 1. INTRODUCTION

Many ocean circulation models assume that temperature and salinity mix at the same rate during turbulence, in that the turbulent diapycnal diffusivities for temperature K_T and salinity K_S are set to be equal (Wells and Griffiths 2003). However, the actual diffusivity ratio $d = K_S/K_T$ seems to depend on the types of fluxes active during turbulence. Specifying the diffusivities correctly is important for General Circulation Models (GCMs), which are three-dimensional mathematical models of the climate system (including the ocean, atmosphere, land, and ice) used to predict climate conditions. Simplified ocean-atmosphere box models are also used to make climate predictions (IPCC 1990). Bryan (1987) examined a numerical ocean GCM and found that it was very sensitive to the magnitude of the vertical diffusivity. Gargett and Ferron (1996) also found that box models of the ocean/atmosphere system are highly dependent on the diffusivity ratio, and changing d by even a factor of two would have a major impact on the results. It is therefore important to understand the mixing behaviors of temperature and salinity. The actual mixing rates of temperature and salinity vary throughout the oceans, as temperature may mix faster in some conditions and salinity may mix faster in other conditions, depending on the stratification and the turbulence of the fluid.

In many locations in the subtropical oceans, the water is stratified such that stable temperature and unstable salinity conditions (henceforth stable-unstable) exist, wherein warm salty water overlies cold fresh water. Under some circumstances this stratification can be conducive to a phenomenon called salt fingers, which cause the salinity at the top to transfer downwards faster than the heat. Salt fingers can form only when the density ratio R_ρ is greater than one, but they are strongest when R_ρ is near one (Schmitt 2003). The density ratio is large when the temperature gradient is large and the salinity gradient is small. It is defined as

$$R_\rho = \frac{\alpha(\partial T / \partial z)}{\beta(\partial S / \partial z)} \ , \tag{1}$$

where α is the thermal expansion coefficient, $\partial T / \partial z$ is the temperature gradient, β is the haline contraction coefficient, and $\partial S / \partial z$ is the salinity gradient. Because salt fingers transfer more salinity than temperature, they cause the salinity gradient to decrease faster than the temperature gradient such that R_ρ increases over time.

Salt fingers are also thought to depend on the turbulence of the fluid. In order to determine how turbulence affects the growth of salt fingers, the turbulence can be characterized by the turbulent Richardson number, defined as

$$Ri_T = \frac{N^2 {L_T}^2}{u^2} \ , \tag{2}$$

where u and L_T are the velocity and length scales, respectively, of the large eddies during turbulence and N is the buoyancy frequency, which is a function of the stratification of the fluid. Ri_T is large when turbulence is weak and it is small when turbulence is strong. The parameter $\varepsilon_a/\nu N^2$, where ε_a is the average dissipation rate during a mixing period and ν is the kinematic viscosity, is commonly used in oceanography to quantify the intensity of the turbulence. $\varepsilon_a/\nu N^2$ is large when turbulence is strong and it is small when turbulence is weak. The relationship between salt fingers and turbulence is still of interest. Taylor (1991), building on the results of Linden (1971), argued that almost any external turbulent event would destroy salt fingers. However, a global ocean model presented by Merryfield et al. (1999) used salt fingers simultaneously with background turbulent diffusivity.

It is also possible that salt finger fluxes could occur at the same time as differential diffusion, although this has not been tested in existing work. Differential diffusion is a phenomenon that has been shown to occur in stable temperature and stable salinity conditions (henceforth stable-stable) during weak turbulence when $Ri_T > 1$ or $\varepsilon_a/\nu N^2 < 300\text{-}500$ (Jackson and Rehmann 2003). It transfers more temperature than salinity and causes the temperature gradient to decrease faster than the salinity gradient such that R_ρ decreases over time. However, if the turbulence is increased so that $Ri_T < 1$ and $\varepsilon_a/\nu N^2 > 300\text{-}500$, temperature and salinity will decrease at approximately the same rate.

The purpose of this study was to determine if differential diffusion fluxes were present during stable-unstable conditions with turbulence. If so, the interaction between salt fingers and differential diffusion was of interest as the levels of turbulence and stratification varied from experiment to experiment. The mixing efficiency during turbulence as conditions were varied was also desired. In order to investigate these points, the following hypotheses were offered:

1. Salt fingers and differential diffusion will both be present during stable-unstable conditions with turbulence. Salt fingers will be stronger when R_ρ is slightly larger than 1 while differential diffusion will be stronger when R_ρ is much larger than 1. In between, there will be a boundary where the fluxes from salt fingers and differential diffusion are equal.
2. Salt fingers and differential diffusion will both be more active during weak turbulence, but will be disturbed by strong turbulence.
3. Mixing efficiency will be higher when differential diffusion fluxes are dominant.

To test these hypotheses, a series of experiments was run with different levels of stratification and turbulence, with the turbulence provided by a system of vertical rods oscillating for a set period of time. Profiles measured after every mixing period were used to compute R_ρ, Ri_T, and other relevant parameters. The changes in R_ρ over the course of each experiment were analyzed to determine if salt fingers, differential diffusion, or neither was dominant. The initial values of R_ρ and Ri_T from each experiment were plotted to create a grid and approximate the regions dominated by salt fingers and differential diffusion. Lastly, a mixing efficiency curve was calculated for each experiment to show how the efficiency changed depending on the levels of stratification and turbulence.

The rest of this thesis details the existing work, the experiments, and the results. Chapter 2 describes the experimental, laboratory, and modeling work that has been done by others. Chapter 3 discusses the experimental facility, the procedures used to prepare for and run experiments, and the calculations used to analyze the results. Chapter 4 describes the results, including a comparison of the initial values of R_ρ and Ri_T from each experiment. It also discusses the behavior of the profiles over the course of each experiment, details the differential diffusion and salt finger regions, and compares the mixing efficiency for each experiment. Chapter 5 summarizes the results and reviews how the findings are applicable to oceanic conditions.

CHAPTER 2. BACKGROUND

2.1 Stable Temperature and Stable Salinity Profiles

In certain locations in the oceans, stable-stable conditions (Figure 1) are present (Merryfield 2002) and are conducive to differential diffusion during periods of weak turbulence. This is possible because the molecular diffusivity of heat D_T is approximately 100 times greater than the molecular diffusivity of salt D_S (Merryfield 2002). Although the turbulent diffusivities for temperature and salinity are significantly greater than their respective molecular diffusivities, K_T will still be larger than K_S for weak turbulence and will cause differential diffusion. For example, during weak turbulence some of the cold salty water below could get displaced into the warm fresh water above. If K_T is greater than K_S, the temperature will transfer faster than the salinity, causing the cold salty water to quickly warm up and become warm and salty, subsequently settling down to between the two layers. This causes the density at the bottom to decrease over time. The diffusivity ratio $d = K_S/K_T$ is less than one when temperature mixes faster than salinity, but it equals one when temperature and salinity mix at the same rates.

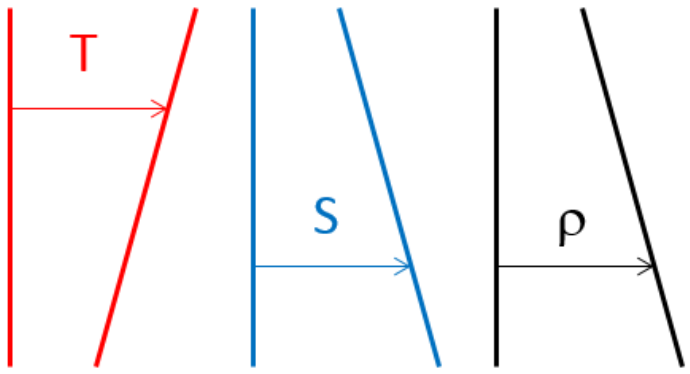

Figure 1. Stable temperature - stable salinity profiles. The density profile is also stable.

Oceanic observations by Merryfield (2002) reported a region in the Arctic Ocean where stable-stable conditions exist. In this region, he observed $0.6 \leq d \leq 0.7$ and 1×10^{-6} m^2/s $\leq K_T \leq 3 \times 10^{-6}$m^2/s. Although this value of K_T is smaller than that measured in other oceans, he argued it is plausible due to the relatively weak turbulence found in the Arctic Ocean. Nash and Moum (2002) also investigated a region with strong turbulence, where differential diffusion would be less likely to occur. The region they studied, located on the Oregon continental shelf, had behavior consistent with differential diffusion, as $d \approx 0.7$.

Two-dimensional numerical simulations by Merryfield et al. (1998) identified conditions where $K_T > K_S$ for weak turbulence, although caution must be exercised in extending the results to three dimensions. Smyth et al. (2005) also studied the turbulent diffusivities of heat and salt using numerical simulations. They found that the diffusivity ratio is typically less than one during the growth and collapse of Kelvin-Helmholtz billows, but will approach one as $\varepsilon_a/\nu N^2$ increases. When $\varepsilon_a/\nu N^2$ is sufficiently small, R_ρ will also affect the diffusivity ratio, as the diffusivity ratio will increase (approaching one) as R_ρ increases (Smyth et al. 2005). Experiments described by Broadwell and Mungal (1991) showed that mixing is affected by molecular diffusivities even in conditions with strong turbulence and large Reynolds numbers.

Jackson and Rehmann (2003) ran experiments to quantify the conditions under which differential diffusion occurs. They found that differential diffusion occurred for $\varepsilon_a/\nu N^2 <$ 300-500 or $Ri_T > 1$, and d varied between 0.5 and 1 for $50 < \varepsilon_a/\nu N^2 < 500$. However, for $\varepsilon_a/\nu N^2 >$ 300-500, they found that $d \approx 1$. Jackson and Rehmann (2003) also investigated how differential diffusion affects the mixing efficiency during turbulence. They defined mixing efficiency R_f as

$$R_f = \frac{\Delta PE}{W} , \tag{3}$$

where ΔPE is the change in potential energy and W is the work done on the fluid during a mixing period. They found that differential diffusion causes an increase in mixing efficiency, which will be larger for large values of Ri_T than for small values of Ri_T. Additionally, they found that when conditions are favorable for differential diffusion ($Ri_T > 1$), mixing efficiency will be greater when the temperature gradient is larger than the salinity gradient, as large values of R_ρ (~5) had higher mixing efficiencies than small values of R_ρ (~0.25), where R_ρ is the negative of the definition provided in Chapter 1, such that it will be positive for stable-stable profiles.

2.2 Stable Temperature and Unstable Salinity Profiles

Stable-unstable conditions (Figure 2) exist in the subtropical oceans because evaporation exceeds precipitation and heating exceeds cooling at the surface (Schmitt 2003). Warm water is less dense than cold water, so when this occurs the temperature profile is stable, as the warm water is at the top. However, salty water is denser than fresh water, so the salinity profile is unstable, as the salty water is at the top. Despite the fact that the salinity profile is unstable with this type of stratification, the overall density profile is stable. This is because R_ρ is greater than 1, meaning that the stability of the temperature keeps the fluid from immediately overturning.

Under the right conditions, the salinity profile will begin to stabilize over time. This happens through a phenomenon called salt fingers (Figure 3), which occur when a series of water cells begin to grow vertically across the stratification and release the potential energy held by the salt towards the top (Schmitt 2003). As they grow, the salinity gradient decreases faster than the temperature gradient, causing the density at the bottom to increase. Because the molecular diffusivity of heat D_T is approximately 100 times as large as that of salt D_S, salt fingers transfer heat laterally without transferring significant salt. In order to grow, salt fingers need a salinity gradient that is only about 1/100 of the temperature gradient, due to the fact that $D_T \approx 100\ D_S$

(Schmitt 2003). Work by Schmitt (1979, 1981, 2003) demonstrated that while salt fingers can form only when R_ρ is greater than one, their growth rate is largest when R_ρ is near one (Schmitt 2003). Additionally, in a model that Merryfield et al. (1999) constructed from previous experimental work on salt fingers, the diapycnal diffusivities causing salt fingers increase as R_ρ approaches one, but are much smaller for $R_\rho > 2$.

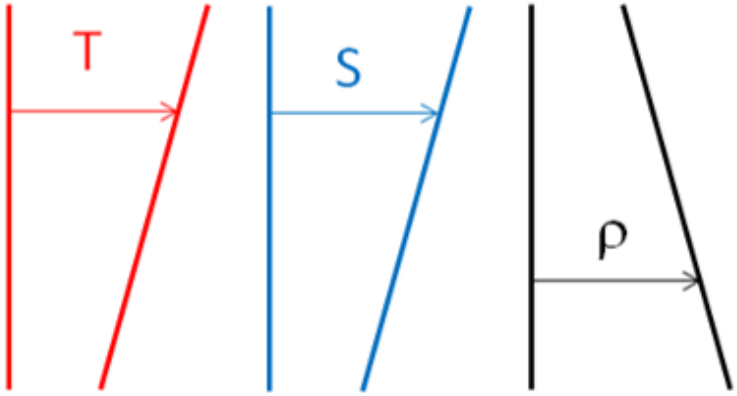

Figure 2. Stable temperature - unstable salinity profiles. The overall density profile is stable.

Figure 3. Salt fingers. As a sample miniature experiment, a cup was initially filled with warm salty colored water on top and cold fresh clear water below (left). After several minutes, salt fingers had formed and colored fingers could be seen growing downwards (right).

Because salt fingers are affected by turbulence, it is important to know how long it takes for salt fingers to form after a turbulent event. The e-folding time can be used as a time scale for the formation of salt fingers and is defined as σ_{max}^{-1}, where σ_{max} is the maximum growth rate (Taylor 1991). The e-folding time is related to the stratification of the fluid, and is large when R_ρ is large. Kunze (1987) defined σ_{max} as

$$\sigma_{max} \cong \frac{1}{2}\sqrt{\frac{(D_T - R_\rho D_S) g \beta (\partial S / \partial z)}{\nu}}(\sqrt{R_\rho} - \sqrt{R_\rho - 1}). \quad (4)$$

where g is acceleration due to gravity. The maximum growth rate defined by Kunze (1987) is half as large as that of Schmitt and Evans (1978) due to different definitions of the salinity gradient term. However, according to Taylor (1991), Kunze's model is applicable to laboratory experiments.

When there is no turbulence present, salt fingers will transfer the salty water at the top downward faster than they transfer the cold water at the bottom upward. Thus, they will cause both R_ρ and the density towards the bottom to increase over time, while the potential energy of the system will decrease over time. When mechanical turbulence is present, turbulent fluxes will also be active. Taylor (1991), building on the results of Linden (1971), argued that salt fingers would be destroyed by almost any external turbulent event. Similarly, Wells and Griffiths (2003) stated that turbulent events would disrupt salt fingers, referencing the work of Linden (1971); however, they also followed the work of Walsh and Ruddick (1995) and noted that turbulent fluxes and salt finger fluxes could be added during periods of intermittent turbulence, with salt finger fluxes growing to a large amplitude after a period of turbulence. A global ocean model presented by Merryfield et al. (1999) for $R_\rho > 1$ also used salt fingers simultaneously with background turbulent diffusivity. Merryfield et al. (1999) used the work of Gargett (1984, 1986), McDougall and Taylor (1984), Zhang et al. (1998), and Schmitt (1981, 1988) to determine the turbulent and salt finger diffusion coefficients. Merryfield et al. (1999) did not consider differential diffusion in these cases, instead assuming that during turbulence the eddy diffusivities of salt and temperature were equal.

For a region with both salt fingers and turbulence, McDougall and Ruddick (1992) examined the magnitudes of salt finger convection and turbulent mixing by determining the dissipation caused by each. The total observed dissipation of mechanical energy ε_{obs} was defined

as the sum of the dissipation caused by salt fingers ε_f and the dissipation caused by turbulence ε_t. These two values could be simply added by assuming that the two mixing types do not change key parameters of the other type, such as the mixing efficiency of internal breaking waves Γ_t. Although studies done by McDougall and Ruddick (1992) and others have accounted for simultaneous salt fingers fluxes and turbulent fluxes, existing work has not yet investigated how salt fingers and differential diffusion interact in stable-unstable conditions or how the resulting overall mixing efficiency is related to the levels of stratification and turbulence.

CHAPTER 3. EXPERIMENTAL FACILITY AND PROCEDURES

3.1 Overview

The experiments were run in a facility that was constructed by Engineering Laboratory Design in the 1990s. The facility features a storage tank, a mixing tank, and a water heater, which are used to prepare the water for the experiments (Figure 4). The water is pumped from the mixing tank to the mixing facility, where experiments are run. The mixing facility (Figure 5) contains a series of combs running lengthwise, which are used to mix the water. Each comb contains thirteen vertical rods. The combs are powered by a motor and oscillate back and forth during mixing. A load cell attached to one of the rods determines the frequency of the combs, which is used to calculate how much work the rods exert on the water. A temperature/conductivity probe is used to profile the water in the mixing facility. The probe is attached to a cart which moves lengthwise on a frame above the mixing facility. The cart contains a stepper motor that moves the probe up and down during a profile. The data obtained from the probe give information on the temperature and conductivity of the water, which can be used to calculate its salinity, density, and potential energy at the time of the profile.

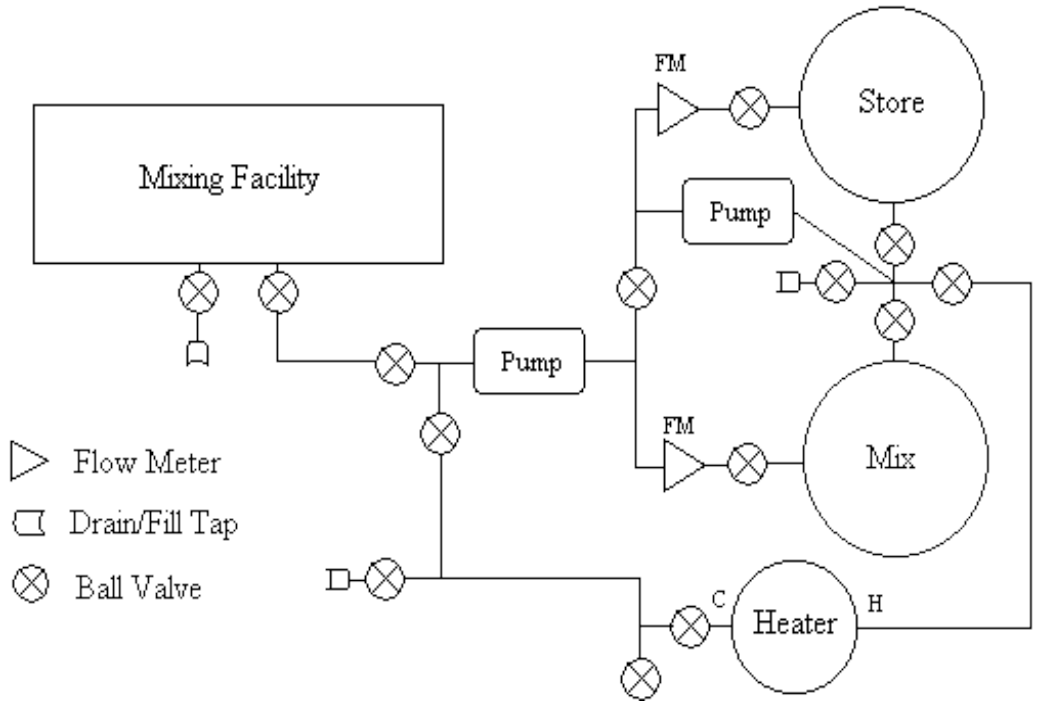

Figure 4. Experimental facility (Jackson 2001).

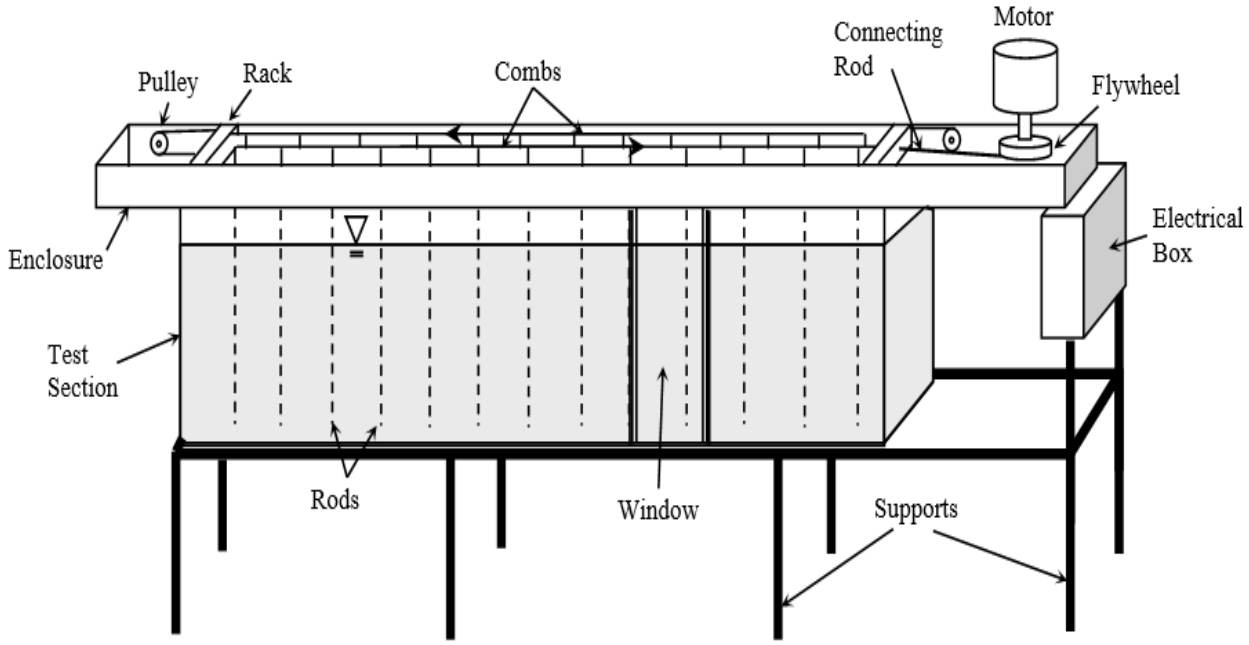

Figure 5. Mixing facility. Only 2 of the 10 comb sets are shown for simplicity (Jackson 2001).

3.2 Experimental Facility

The experiments were performed in the mixing facility, a tank made out of fiberglass reinforced plastic and rigid PVC foam core material. It is 2 m long, 0.4 m wide, and 0.6 m deep. It has a 0.25 m wide transparent Plexiglas viewing window built into each side that is used to make sure that the water inside is filled to the desired height and that the probe is used correctly. The windows are located approximately 60 cm from one end of the tank. Water enters the mixing facility in the middle of the bottom, and is met by a 25 cm by 35 cm Plexiglas diffuser plate, which ensures the water flows in horizontally, as vertical flow would disrupt the desired stratification. The mixing facility is covered by a removable 1.9 cm-thick Plexiglas top, which has a 0.95 cm wide slot running down the full 2 m length. The entire slot is fitted with nylon brushes to reduce air flow through the slot, except at one point near the viewing windows, where a small gap is left for the insertion of the probe.

Water in the mixing facility is mixed by an assembly of ten combs, which oscillate back and forth along the length of the facility at a stroke length of 7.5 cm and a frequency of 0 to 0.10 Hz. Neighboring combs oscillate 180 degrees out of phase to prevent mean flows from being generated inside the facility. Each comb contains thirteen vertical fiberglass rods spaced 15 cm apart. Each rod is 1.27 cm by 1.27 cm and 60.0 cm long, extending from above the surface of the water (which had a target depth of 50 cm above the bottom during experiments) down to near the bottom of the mixing facility. Above the diffuser plate, three rods on each comb are shortened to 57.9 cm so that they do not hit the plate. The combs are spaced 4 cm apart on center across the width of the facility and are kept at the correct spacing by several Plexiglas strips, which are each attached to the tops of three combs moving at the same phase. The combs are also guided on each end of the length of the facility by aluminum racks. The length scale L_T of the large eddies

during turbulence, which is used to calculate Ri_T, is set to the 4 cm distance between the combs (Martin and Rehmann 2006).

The combs are powered by a flywheel and pulley system that is driven by a 0.5 hp motor. This assembly allows the combs to be oscillated between 0 and 60 RPM. The frequency of the mixing combs is controlled by a variable speed motor control mounted on the side of the mixing facility, which adjusts the frequency in increments of approximately 0.1 RPM. The frequency was set to a selected constant level before each experiment. A load cell attached to one of the rods determines the actual frequency of the combs. The cover, sides, and bottom of the mixing facility are all covered with at least 3 cm of Styrofoam insulation to reduce heat loss from the water inside. The viewing windows are also covered with insulation panels, but these are easily removable for observation. The surface of the water is also covered with approximately 10 cm of 0.75 cm diameter Styrofoam beads. When the mixing facility is filled to its target depth of 50 cm during an experiment, the beads fill up most of the area between the surface of the water and the underside of the mixing combs.

The mixing facility is connected to the storage and mixing tanks by a network of PVC pipes and valves. Two 348-liter Raven Model K2563 vertical insulated tanks were used to store the water and ensure that it was at the desired temperature and salinity before being pumped into the mixing facility. The tanks each have a height of approximately 140 cm and an inside diameter of approximately 60 cm. A Neptune Model A-1 mixer is placed on top of each tank. These mixers rotate at 1725 RPM and are mounted at about 9 degrees off vertical in order to avoid causing large vortices. The mixer shafts are 101 cm long and 1.27 cm in diameter, with an impeller of approximately 10 cm diameter on the ends.

A 151-liter electric water heater is connected to both tanks through the pipe network, which allows both to be heated to the desired temperatures. Flow between the tanks, the water heater, and the mixing facility is powered through the use of two March Model AC-2CP-MD 5 GPM (0.32 liter/s) pumps, which pump from the bottom of the tanks. The approximate flowrate out of each tank is measured using two Blue-White flowmeters, which measure flowrates from 0 to 5 GPM (0 to 0.32 liter/s).

3.3 Measurement Instruments

During the experiments, a Model 125 MicroScale Conductivity-Temperature Instrument (MSCTI) from Precision Measurements Engineering was used to measure the temperature and conductivity profiles. These profiles were then used to calculate the salinity profile, density profile, and potential energy of the fluid at the time the profile was taken. The MSCTI includes a probe and a bridge box. The probe measures temperature using a FP07 thermistor with a 7-millisecond response time. It also measures conductivity using a sensor that passes an electric signal between four elements. The thermistor and conductivity sensor are at the tip of a narrow stainless steel rod, which passes through the water with minimal disturbance. A glass tube placed around the outside of the probe protects the tip from the Styrofoam beads as it passes through them. Before a profile is taken, however, the glass tube is slid up above the tip so that it does not interfere with the readings. The profiles collected by the probe are passed along in the form of voltage signals through the bridge box and to the data acquisition (DAQ) unit.

In order to take profiles, the probe is clamped to a Velmex positioning system, which moves up and down through the water at a speed of 20 mm/s. The Velmex system contains a stepper motor that can be controlled by a computer through a serial port. A LabVIEW code is used to make the Velmex system control the movement of the probe, including its direction,

speed, and acceleration. The Velmex system is attached to a cart that moves lengthwise along the entire 2 m length of the mixing facility. The cart travels on a stand-alone frame made out of square steel tubing. The frame is placed over the top of the mixing facility but is independent from its structure and can be leveled separately. The position of the probe within the clamps can also be adjusted to ensure that it is level and takes vertical profiles.

The voltage signals from the probe and the load cell are read by a data acquisition (DAQ) unit from Measurement Computing (USB-1608G). The DAQ contains 8 differential analog inputs, 2 of which are used to read the temperature and conductivity data from the MSCTI, and one of which is used to read the data from the load cell. After the DAQ reads the signals, it passes them along to a computer where LabVIEW programs read the raw voltage data and convert it into temperature, conductivity, salinity, and density profiles, which are used to calculate the potential energy of the mixing facility at that time.

In order to calculate the work done on the water by the vertical rods, the frequency of the mixing rods during each stirring period was determined. To identify the frequency f, a load cell (LBB200) made by Futek Technologies was placed in a gap in one of the rods. The load cell contains a strain gage to convert material deformation to positive or negative electrical signal. As the rod oscillates through the water, the load cell outputs a sinusoidal voltage signal which is read and plotted. That signal was then fit to an equation of the form

$$V = A \cdot sin(\omega \cdot t), \tag{5}$$

where V is the voltage signal in volts, A is the amplitude of the signal in volts, ω is the frequency in rad/second, and t is the time in seconds. For each stirring period, ω was then converted to f in cycles/s and f was used to calculate the work done as described in section 3.6.2.

The initial voltage to the load cell is provided by a Programmable Power Supply PPS2116A made by Circuit Specialists. This power supply can output an adjustable voltage of 0 to 32 VDC at a current of 0 to 5 A, but during experiments it was set so that it output approximately 7.0 V and 0.015 A. The voltage travels out of the power supply, through an amplifier/conditioner (made by Tacuna Systems), and to the load cell. The load cell has a rated voltage signal of 1 mV/V and outputs a sinusoidal voltage signal that goes back through the amplifier/conditioner, where a potentiometer was used to adjust the average output to approximately 2.5 V. The amplifier/conditioner amplifies the signal and removes noise above 180 Hz, before passing along the voltage to the DAQ. A separate LabVIEW program applies a low-pass Butterworth filter with a low cutoff frequency of 0.23 Hz to the load cell data to remove high frequency noise and oscillations. Each of the stirring periods had a frequency of less than 0.10 Hz, so the low-pass filter allowed the voltage signal from the mixing to pass, but filtered out the high frequency noise above 0.23 Hz.

3.4 Procedures

3.4.1 Calibrations

The calibration procedures for the thermistor and conductivity sensor are described in the following sections. Although not identical, they are closely based on the procedures described by Jackson (2001).

3.4.1.1 Thermistor

The thermistor was calibrated prior to the beginning of each experiment. To calibrate the thermistor, fresh water samples at different temperatures were prepared. Typically, temperatures of about 15°C to 27°C were used, as this covered the temperature range of the water in the tanks

and the mixing facility during the experiments. Samples were spaced out approximately every 3°C. The voltage values from the probe were read by the MSCTI, passed along to the DAQ, and then read by a computer using either LabVIEW or Instacal. Additionally, before any samples were read during calibration, the probe was disconnected from the MSCTI, the MSCTI was turned off, and the voltage of its temperature port was recorded as V_{toff}.

After turning the MSCTI back on and reconnecting the probe, the tip of the probe was placed in a water sample, along with the sensor of a NIST Certified Traceable® Platinum Ultra-Accurate Digital Thermometer. The temperature from the thermometer was then recorded simultaneously with the probe voltage (V_t), using the computer program Instacal. This process was repeated until all of the temperature points had been covered, and an equation of the form

$$V_t - V_{toff} = c \cdot e^{d/T} \tag{6}$$

was fit to the data (Figure 6), where T is temperature in K and c and d are coefficients. The parameters c, d, and V_{toff} were then used in LabVIEW to calculate the temperature for each V_t, using the rearranged equation

$$T = \frac{d}{\ln\left(\frac{V_t - V_{toff}}{c}\right)}. \tag{7}$$

As a check, the V_t values from the calibration were inserted into the equation to make sure that the results from the equation matched the actual temperature values given by the thermometer during calibration. If all of the calibration points that were within the temperature range for an experiment were within +/- 0.06 °C, then the thermistor calibration was a success.

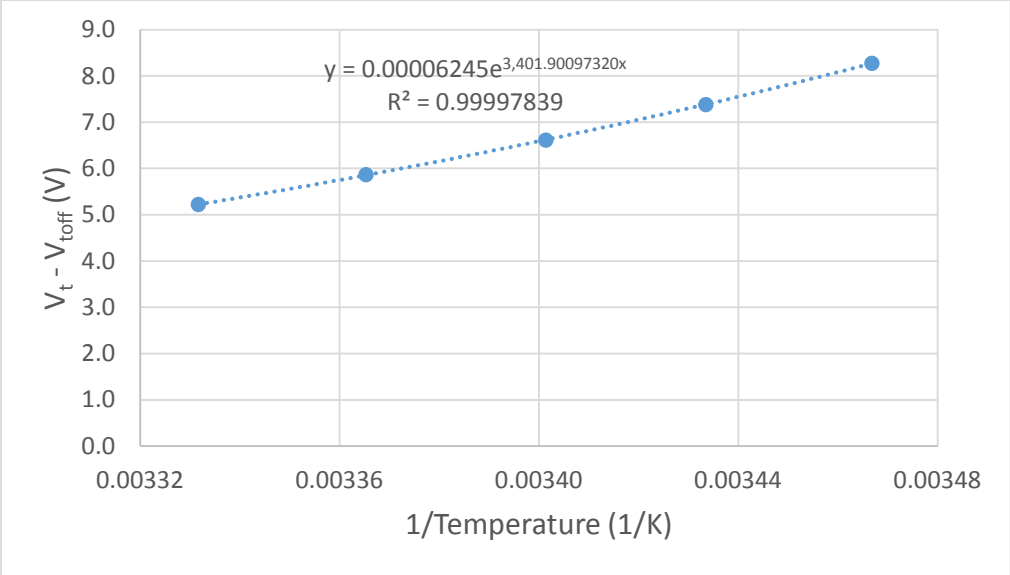

Figure 6. Sample thermistor calibration curve.

3.4.1.2 Conductivity Sensor

The conductivity sensor was also calibrated prior to the beginning of each experiment. To calibrate the conductivity sensor, seven solutions of known salinity were mixed, ranging from 0.00% to approximately 0.30%, as this covered the salinity range of the water in the tanks and the mixing facility during the experiments. Samples were spaced out approximately every 0.05%. The actual precise salinity values of the samples were calculated using the following equation:

$$\text{Salinity}\ (\%) = 100 \cdot \frac{\text{Mass}_{salt}}{\text{Mass}_{salt} + \text{Mass}_{water}}. \tag{8}$$

The samples were well mixed and the tip of the probe was placed in a sample. A LabVIEW program simultaneously read the voltage due to conductivity V_c and the voltage due to temperature V_t. The temperature for that sample was then calculated using the coefficients found for that experiment during the thermistor calibration, as described in section 3.4.1.1. The

calculated salinity value for that sample was also recorded. This process was repeated until all of the salinity points had been covered.

After the temperature and salinity values for all of the samples had been found, a MATLAB program was used to calculate the conductivity of each sample, using the process described by Rehmann (1995). For each sample, V_c was then plotted against conductivity and a linear trend line was fit to the points (Figure 7). The linear trend line is of the form

$$V_c = G_c\sigma + V_{coff}\,, \tag{9}$$

where σ is conductivity in mS/cm and G_c is a coefficient. This equation was rearranged as

$$\sigma = \frac{V_c - V_{coff}}{G_c}\,, \tag{10}$$

and used in LabVIEW to calculate conductivity for each V_c when given G_c and V_{coff}.

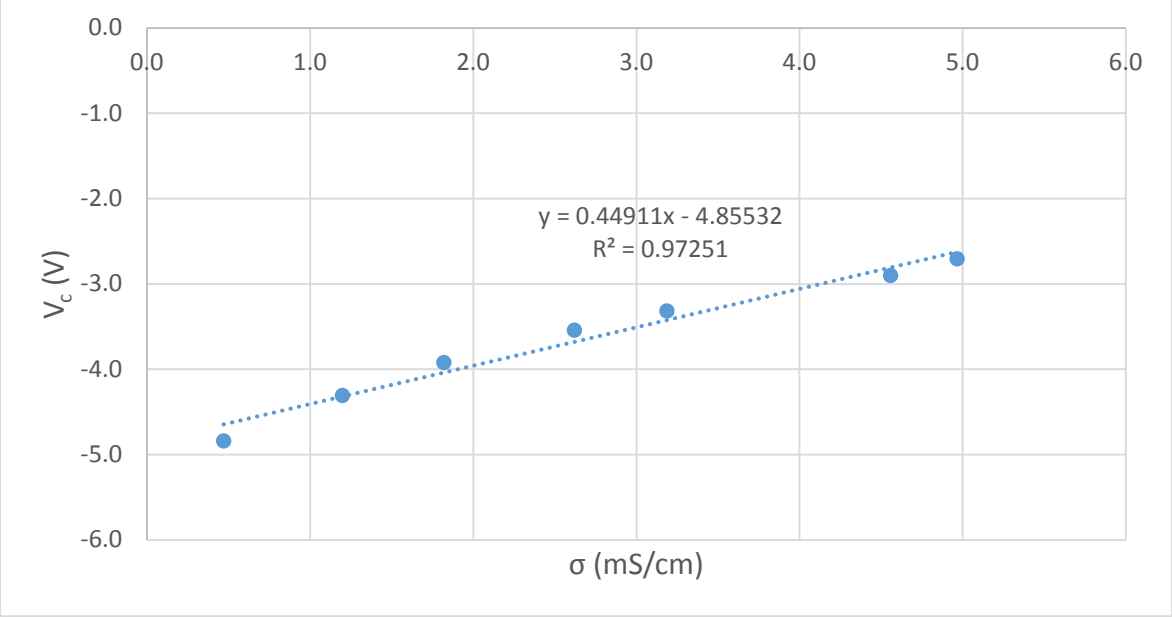

Figure 7. Sample conductivity calibration curve.

3.4.2 Stratification

The experiments were run using the double bucket method for stratification. This is done by filling the storage and mixing tanks, heating them by pumping water through the water heater, placing salt in them if necessary, and mixing until each is at the desired temperature and salinity. While the water in both is continuously mixing, the water is pumped out of the bottom of the storage tank and into the top of the mixing tank, and then out of the bottom of the mixing tank and into the bottom of the mixing facility.

Because the desired profiles for the mixing facility for these experiments are warm salty water over cold fresh water, the water in the mixing tank is made warm and salty, while the water in the storage tank is made cold and fresh. When filling begins, the warm salty water from the mixing tank is the first water to be placed into the mixing facility, so it rises to the top as the mixing facility fills. As the cold fresh water from the storage tank flows into the mixing tank, the water in the mixing tank begins to become less warm and salty. Subsequently, as the mixing facility fills, the temperature and salinity of the water entering it from the bottom gradually changes. When the mixing facility is at its desired depth and filling is complete (with both of the pumps turned off and all of the valves closed), it has warm salty water at the top and colder fresher water at the bottom.

In order to get the desired linear temperature and salinity profiles in the mixing facility, the proper pumping flowrates must be set. Let V_1, S_1, and T_1, be the volume, salinity, and temperature, respectively, of the storage tank and let Q_1 be the flowrate out of the storage tank into the mixing tank. Let V_2, S_2, and T_2, be the volume, salinity, and temperature, respectively, of the mixing tank and let Q_2 be the flowrate out of the mixing tank into the mixing facility.

To find the salinity and temperature in the mixing tank as a function of time, the conservation equations for salt, heat, and volume in the mixing tank must be set:

$$\begin{aligned} \frac{d}{dt}(S_2V_2) &= S_1Q_1 - S_2Q_2 \\ \frac{d}{dt}(T_2V_2) &= T_1Q_1 - T_2Q_2 \\ \frac{dV_2}{dt} &= Q_1 - Q_2 \end{aligned} \quad . \tag{11}$$

If $S_2(0) = S_{20}$, $T_2(0) = T_{20}$, and $V_2(0) = V_{20}$, then the differential equations can be solved to find the salinity and temperature in the mixing tank as a function of time:

$$\begin{aligned} S_2(t) &= S_1 + \frac{(S_{20} - S_1)(V_{20})^{\frac{Q_1}{Q_1-Q_2}}}{(V_{20} + (Q_1 - Q_2)t)^{\frac{Q_1}{Q_1-Q_2}}} \\ T_2(t) &= T_1 + \frac{(T_{20} - T_1)(V_{20})^{\frac{Q_1}{Q_1-Q_2}}}{(V_{20} + (Q_1 - Q_2)t)^{\frac{Q_1}{Q_1-Q_2}}} \end{aligned} \quad . \tag{12}$$

If $Q_2 = 2Q_1$, then the salinity and temperature in the mixing tank will change linearly as a function of time:

$$\begin{aligned} S_2(t) &= \frac{Q_1(S_1 - S_{20})t}{V_{20}} + S_{20} \\ T_2(t) &= \frac{Q_1(T_1 - T_{20})t}{V_{20}} + T_{20} \end{aligned} \quad . \tag{13}$$

Because the water in the mixing tank is the water that is pumped into the mixing facility, this will yield linear salinity and temperature profiles in the mixing facility.

3.5 Temperature and Conductivity Measurements

The mixing facility was filled to a target depth of 50 cm in each experiment, although the depth was sometimes not exactly 50 cm because the Styrofoam beads at the surface of the water made it difficult to set the depth to exactly 50 cm. After the mixing facility was filled, initial temperature and conductivity profiles were measured and additional profiles were taken after every 20 minute (+/- 12 sec) stirring period. The profiles were taken by placing the tip of the probe approximately 10 mm below the Styrofoam beads floating on the surface of the water so that the beads did not interfere with the probe readings. The Velmex was then used to lower the probe at a speed of 20 mm/s and data points were collected every millimeter until it was approximately 20 mm above the bottom of the mixing facility. The initial profile had its first point at a height of 499 mm above the bottom, but because the Styrofoam beads would rearrange after the first stirring period, most subsequent profiles had their first points at 489 mm above the bottom so that the beads would not interfere with the probe readings. The stratification of the tank was assumed to be uniform throughout, so the profiles were taken near the viewing windows so that it could be ensured that the probe was set up correctly.

The initial profiles were taken soon after filling and all subsequent profiles were taken soon after mixing and before salt fingers had fully formed so that it could be determined if differential diffusion or salt finger fluxes were stronger during mixing. Before each experiment, the e-folding time, which serves as an approximation of the formation time for salt fingers, was calculated for the proposed conditions for that experiment. By calculating the e-folding time for each experiment, it was possible to make sure that profiles were taken after each stirring period before one e-folding period had elapsed. After the experiments were run and the data had been processed, the actual e-folding times were calculated and compared to the amount of time it took

to take the profiles after mixing. In all cases, the profiles were taken within or slightly after one e-folding period had elapsed.

3.6 Data Processing and Calculations

3.6.1 Temperature and Conductivity

After the temperature and conductivity profiles were read from the MSCTI, a LabVIEW program calculated the salinity and density profiles. The salinity and density were calculated using the process described by Jackson (2001). The temperature and salinity profiles were then analyzed and any significant abrupt multipoint irregularities at the top and bottom were identified. Those segments were removed from the density profiles, and the remaining points were used. Major density instabilities at the top of the density profiles, likely caused by salt sticking to the Styrofoam beads at the surface, were also removed from the profiles. A MATLAB program was then used to extend the density profiles to the top (z = 500 mm) and bottom (z = 0 mm). The top and the bottom were analyzed separately by fitting a parabola to each end of the profile. The parabolas were fit by analyzing a given number of points and matching the value and slope at the existing end points (Rehmann and Koseff 2004). The parabolas were set to be vertical at the top and bottom so that the profiles behaved as if there were no flux at the boundaries.

An interior section of each profile, extending from a depth of 100 mm to a depth of 400 mm, was used to calculate the temperature and salinity gradients. This portion of the profiles was used because it was the most linear section of the profiles, typically with a linear fit of $R^2 > 0.9$. The temperature and salinity gradients were then used to calculate R_ρ. The uncertainty for each value of R_ρ was found by statistically analyzing how closely the linear trend lines fit the data

using a 95% confidence interval, following the process described by Morrison (2014). Additionally, the density profiles were used to calculate the potential energy for each profile. Potential energy E_p was defined as

$$E_p = g \cdot L \cdot B \cdot \int z \cdot \rho dz, \tag{14}$$

where L is the length of the mixing facility, B is the width of the mixing facility, z is the vertical position, and ρ is the density.

3.6.2 Work

The work W was calculated using the process described by Martin and Rehmann (2006). They approximate the work during each stirring period as the product of the mean force F, the maximum rod velocity U_m, and the stirring time T_{stir}:

$$W = FU_m T_{stir} = \frac{N_r L_r \rho_0 C_d d_r}{4} S^3 \pi^3 f^3 T_{stir}, \tag{15}$$

where N_r is the total number of rods, L_r is length of the submerged portion of a standard rod, ρ_0 is the average density of the fluid during mixing, d_r is the length of the side of a rod, and S is the stroke length. The rods over the diffuser plate are considered to be a proportional portion of a rod, since they are slightly shorter than the full-length rods. The drag coefficient C_d was set to 2.06, as Martin and Rehmann (2006) determined it to be 2.06 ± 0.02 for this mixing facility.

3.6.3 Mixing Efficiency

The mixing efficiency η of the system during an experiment was found from the potential energies calculated for each profile using a process similar to that of Wykes and Dalziel (2014). For each profile, the background potential energy E_b was also found, which is the minimum

energy state possible for that experiment. This would occur under adiabatic conditions if the fluid parcels were allowed to rearrange vertically without mixing until in equilibrium. This was found by taking density profiles and sorting them so that they were completely stable, with the smallest densities at the top and the largest densities at the bottom.

Because E_b is the minimum adiabatic potential energy possible at the time of a profile, the available potential energy E_a of each profile is then the difference between E_p and E_b. In order to show how efficiently the work applied to the system during mixing changes the potential energy as compared to its initial condition, the mixing efficiency was computed as

$$\eta = \frac{\Delta E_b}{\Delta E_a + W}, \tag{16}$$

where Δ describes the change in energy between the initial profile of the experiment and the profile being examined. W is the total amount of work up to that point in the experiment that has been exerted by the rods on the fluid during mixing. If the potential energy of the system increases by the same amount as the work put into the system, η will equal 1. However, if the potential energy of the system increases by less than the amount of work put into the system, η will be less than 1.

CHAPTER 4. RESULTS

4.1 Density Ratio and Turbulent Richardson Number

A series of experiments was run (Table 1) to create a grid of points with different values of R_ρ and Ri_T (Figure 8). Initially, four experiments were planned to map out the area of interest and identify observable trends. The four points (experiments SF_3, DD_2, SF_1, and DD_3) either had a low (~2) or a high (~5) initial R_ρ ($R_{\rho 0}$) and either a low (~0.7) or a high (~2.1-2.4) initial turbulent Richardson number Ri_{T0}. In addition to mapping out the four corners and observing the behavior of the profiles, three more experiments were run in order to get more information about the behavior of the profiles. The first point (experiment DD_1) was similar to experiment DD_2, as it again had a high Ri_T (~2.5), but it had a slightly lower R_ρ (~4). The second point (experiment SF_4) was between experiments SF_1 and SF_3, as it had a low R_ρ (~2) and a mid-range Ri_T (~1.4). The last point (experiment SF_2) was closer to the center of the grid, with mid-range values of R_ρ (~3) and Ri_T (~1.6).

Table 1. Experiment Parameters.

Experiment	Initial f (Hz)	Initial N (rad/s)	$R_{\rho 0}$	Ri_{T0}	Initial $\varepsilon_a/\nu N^2$	Initial e-folding time (s)
SF_1	0.028	0.09	1.81	2.4	39.2	125.8
SF_2	0.051	0.13	2.83	1.6	108.6	169.8
SF_3	0.050	0.09	1.62	0.7	227.4	99.7
SF_4	0.035	0.09	1.87	1.4	83.1	135.2
DD_1	0.041	0.13	4.21	2.5	54.4	278.6
DD_2	0.050	0.15	5.13	2.1	79.9	320.8
DD_3	0.085	0.14	4.91	0.7	424.4	313.4

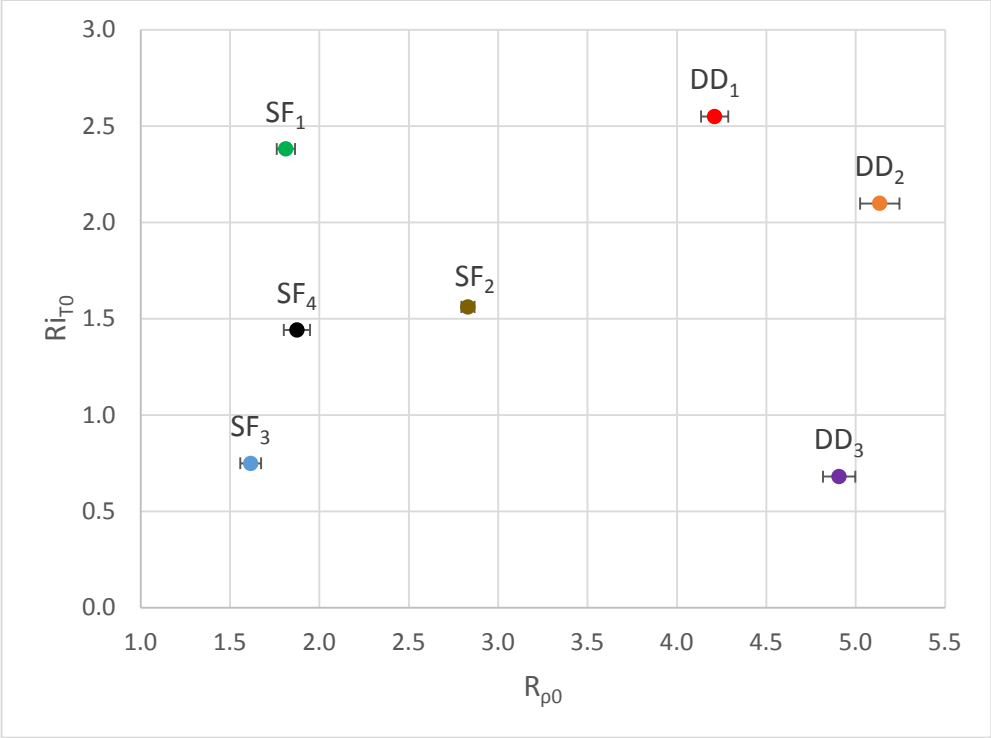

Figure 8. Initial Ri_T vs. initial R_ρ.

4.2 Evolution of the Profiles

Seven profiles were recorded for each experiment. Each profile was taken soon after the end of filling or mixing and typically before one e-folding period had elapsed, in an effort to try to ensure that new salt fingers had not yet become established after turbulence and begun to significantly change the profiles. Even so, the profiles were not taken immediately after mixing, and mixing was not restarted immediately after a profile was taken, thus in essence modeling intermittent turbulence. Consequently, the profiles reflect what happened not only during mixing but also during the time between mixing periods. Even if the turbulence disturbed most of the salt fingers, there was opportunity for at least some salt finger growth by the time the profiles were taken, and fingers could continue to grow undisturbed after a profile until the next mixing period started. Because profiles had to be taken promptly, turbulence was not given time to decay, as was practice in stable-stable experiments by Jackson and Rehmann (2003). Thus, the profiles occasionally contained fluctuations that were likely due to salt fingers and/or residual turbulence.

For each experiment, the density profiles evolved over time, with the initial profiles containing a larger range of densities than the final profiles. The density profiles for all of the experiments had approximately the same evolution over time, although the exact behaviors were slightly different for experiments dominated by differential diffusion (Figure 9) and those dominated by salt fingers (Figure 10). Throughout the evolution of the profiles, mass was conserved by at least 99.9965% for each experiment. When the experiments started with a large R_ρ, the temperature gradient decreased faster than the salinity gradient over time, as is evident in the slight clockwise rotation of the temperature-salinity diagrams (Figure 11). When the experiments started with a small R_ρ, the salinity gradient decreased faster than the temperature

gradient over time, as is evident in the counterclockwise rotation of the temperature-salinity diagrams (Figure 12). The temperature-salinity diagrams are plotted using only the interior linear portions of the profiles.

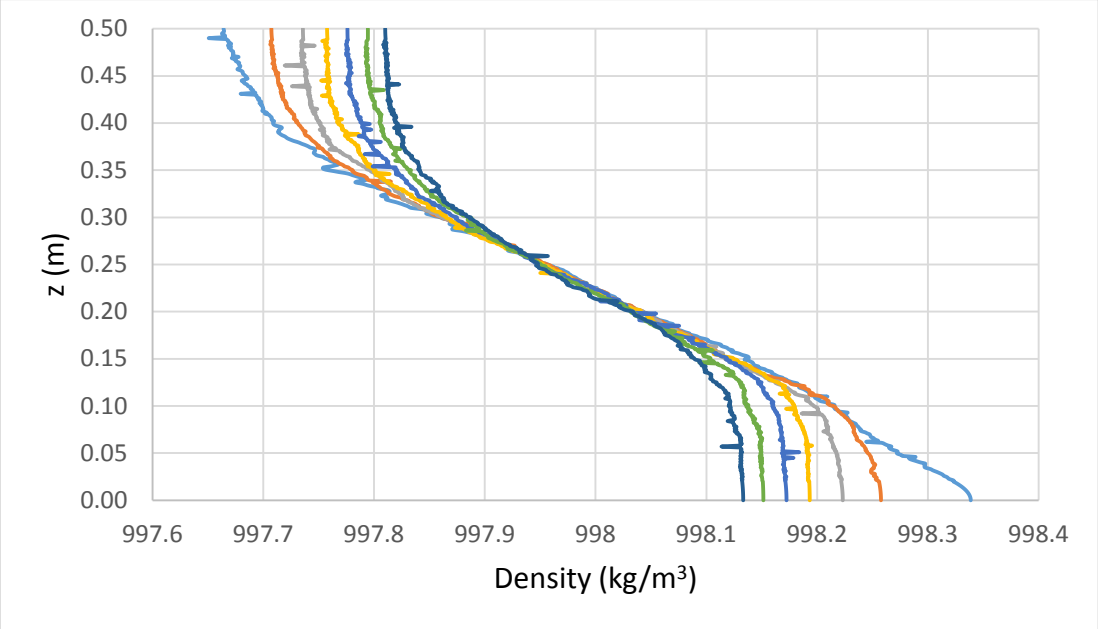

Figure 9. Standard density profile evolution for differential diffusion. This one was taken from experiment DD_1.

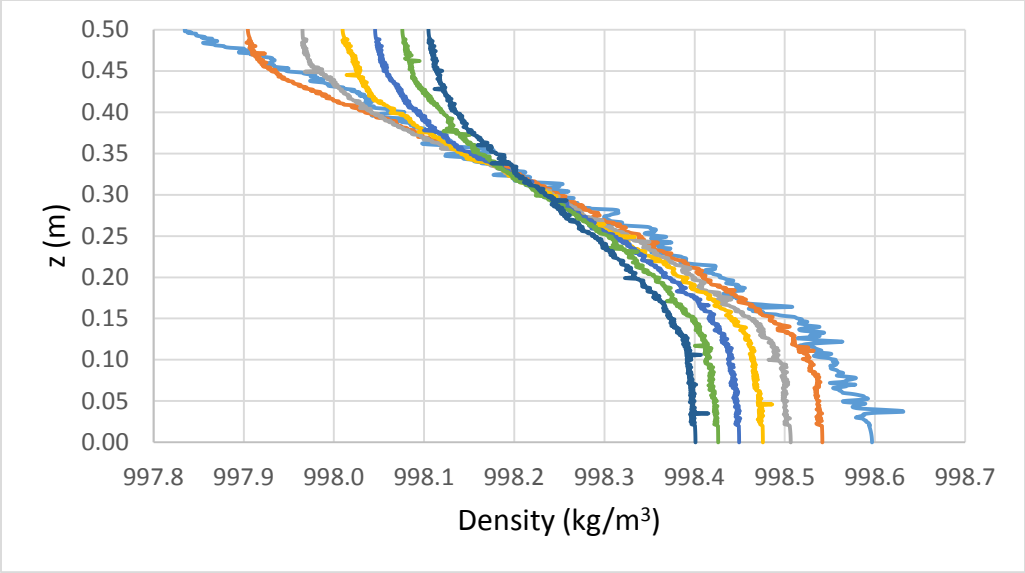

Figure 10. Density profile evolution for salt fingers experiment SF_2. The profile evolutions varied between salt fingers experiments, but all of them generally condensed over time.

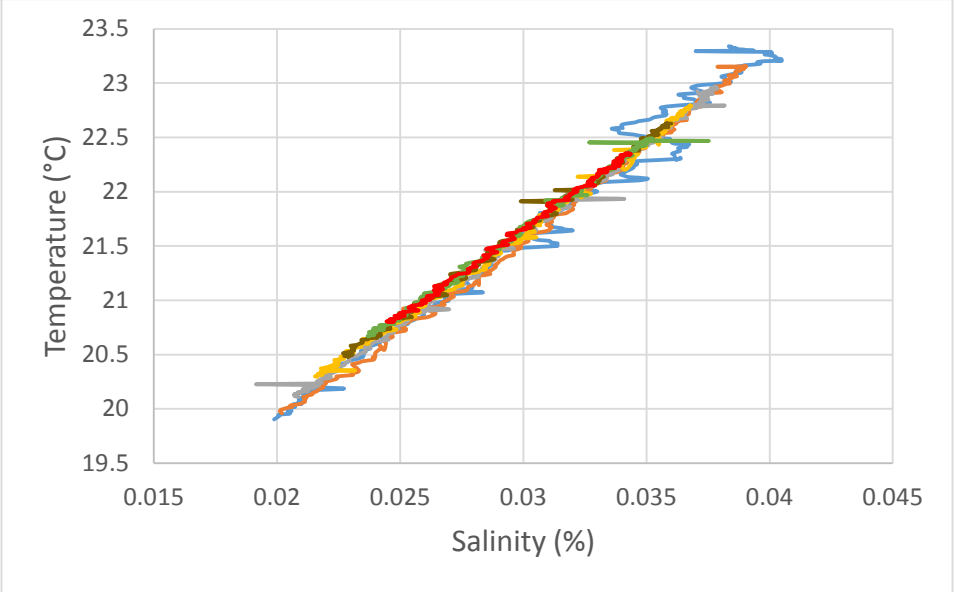

Figure 11. Standard temperature-salinity diagram for differential diffusion dominated experiments. This one was taken from experiment DD_2. The blue line is from the initial profile and the red line is from the final profile. Note the slight clockwise rotation and that ΔT and ΔS both decrease over time.

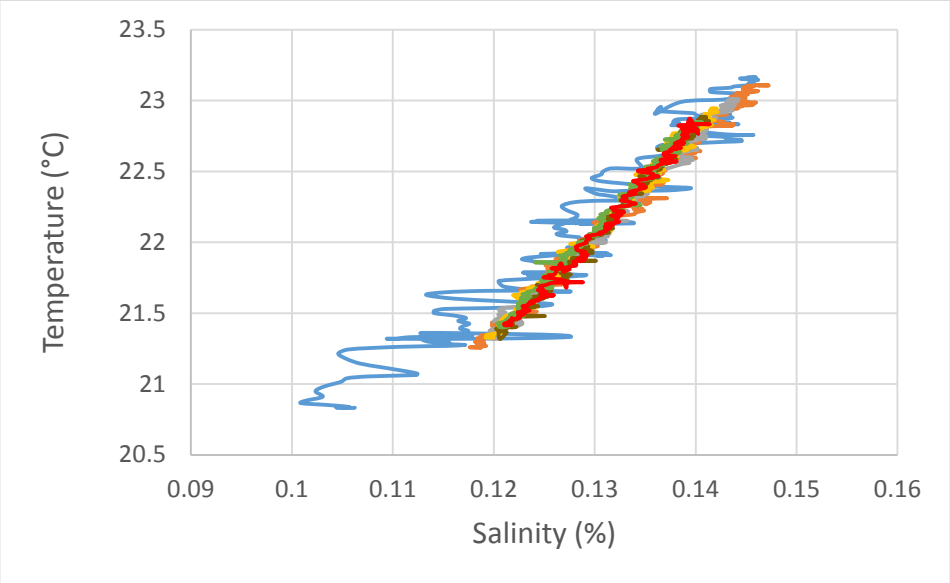

Figure 12. Standard temperature-salinity diagram for salt finger dominated experiments. This one was taken from experiment SF_1. The blue line is from the initial profile and the red line is from the final profile. Note the slight counterclockwise rotation and that ΔT and ΔS both decrease over time.

4.3 Salt Finger and Differential Diffusion Regions

The behavior of the fluxes during the experiments was largely dependent on the stratification of the fluid. When the experiments began with a large R_ρ, differential diffusion was dominant, and R_ρ decreased slowly over time (Figures 13 and 14). When the experiments began with a small R_ρ, salt fingers were dominant, and R_ρ rose steadily over time (Figures 13 and 14). This behavior agrees with the work of Merryfield et al. (1999), who found that salt fingers fluxes were typically stronger when R_ρ was closer to 1. When uncertainty bars are added to R_ρ, the results in Figures 13 and 14 show that R_ρ seems to be clearly increasing over the course of experiments SF_1, SF_2, SF_3, and SF_4. R_ρ seems to be slightly decreasing over the course of

experiments DD_1, DD_2, and DD_3, but $R_\rho / R_{\rho 0} \geq 1$ is within the uncertainty range for all three experiments in Figure 14.

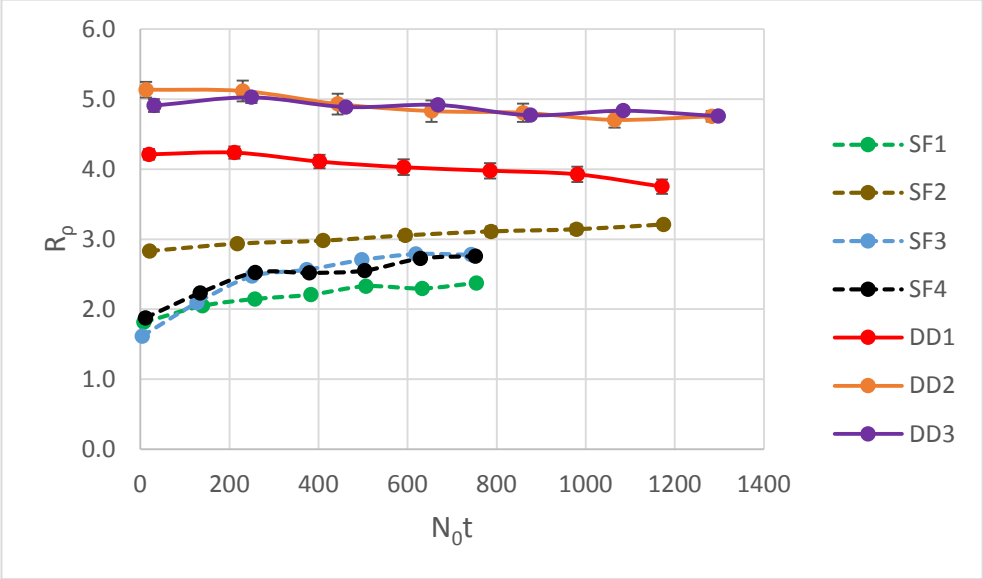

Figure 13. R_ρ vs. N_0t. N_0 is the initial buoyancy frequency. Experiments with a large initial R_ρ have solid lines and experiments with a small initial R_ρ have dashed lines.

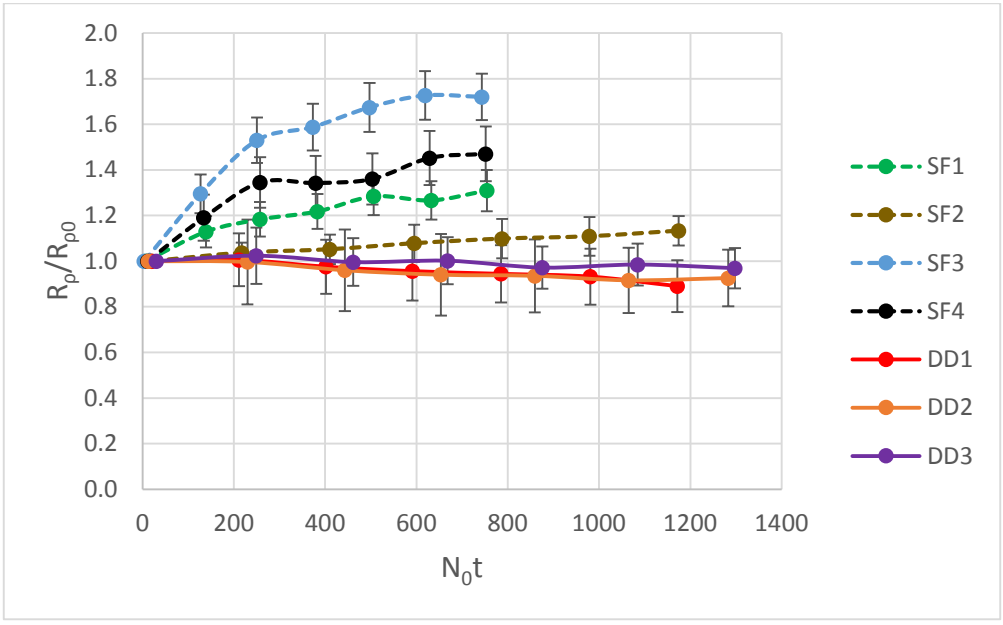

Figure 14. $R_\rho/R_{\rho 0}$ vs. N_0t.

Turbulence also influenced the behavior of the profiles. Jackson and Rehmann (2003) found that differential diffusion occurs for light mixing when $\varepsilon_a/\nu N^2 < 300\text{-}500$ or when $Ri_T > 1$. Although the initial $Ri_T < 1$ for two of the experiments (Figure 8), in all seven experiments the initial $\varepsilon_a/\nu N^2 < 500$ (Figure 15), so conditions were at least somewhat conducive to differential diffusion. However, in experiments DD_2 and DD_1, R_ρ decreased more significantly than in experiment DD_3, even though all three began with similar values of R_ρ. This is likely because there was weaker turbulence and therefore a smaller initial $\varepsilon_a/\nu N^2$ (<80) and a larger Ri_T (>2) in experiments DD_2 and DD_1 as compared to experiment DD_3 (initial $\varepsilon_a/\nu N^2$ of 424 and initial Ri_T of 0.7).

Originally, it was expected that strong turbulence in the salt finger favorable region would minimize differential diffusion and overpower all salt finger fluxes, making R_ρ remain mostly constant. However, profiles taken after strong mixing in the salt finger favorable region (experiment SF_3) showed that R_ρ actually increased more over time than when profiles were taken after weak mixing in that region (experiment SF_1), indicating that salt finger fluxes were active during and/or after strong mixing. Experiment SF_4 also supported this conclusion, as it experienced more turbulence than experiment SF_1 and less turbulence than experiment SF_3, but its R_ρ increased faster than R_ρ increased during experiment SF_1 and slower than R_ρ increased during experiment SF_3.

The increase in R_ρ during strong turbulence may be due in part to the fact that some time elapsed between the end of the mixing periods and the time when profiles were taken (values varied between 83 and 205 seconds). Although this time period was almost always shorter than the e-folding period, indicating that salt fingers were still becoming established, they still could have begun raising R_ρ. For both weak and strong turbulence, salt fingers also could have grown

in the periods of time between when the profiles were taken and when the next mixing periods began (values varied between 72 and 139 seconds), which also would have increased R_ρ.

It is also possible that salt fluxes were at least somewhat active during mixing. This agrees with the work of Merryfield et al. (1999), who used salt fingers and other turbulent diffusivities simultaneously in their model. During strong mixing (experiment SF_3) differential diffusion fluxes would be weak, so if there were any salt finger fluxes, R_ρ could start to rise. Between mixing periods salt fingers would continue to grow, presumably leading to a large increase in R_ρ when profiles were taken. During weak mixing (experiment SF_1) differential diffusion fluxes would be stronger, so they would counteract any preferential transport of salt by salt finger fluxes, making R_ρ decrease or remain basically constant. Between mixing periods salt fingers would grow, presumably leading to a moderate increase in R_ρ when profiles were taken.

Salt fingers are clearly stronger than differential diffusion in experiments SF_1, SF_2, SF_3, and SF_4 (Figure 14), so there is a region on the left of Figure 8 where salt fingers dominate. In experiments DD_1, DD_2, and DD_3, differential diffusion appears to be stronger than salt fingers. However, $R_\rho / R_{\rho 0} \geq 1$ is within the uncertainty range for all three differential diffusion experiments in Figure 14, so it cannot be definitively stated that differential diffusion would dominate the region on the right of Figure 8. Nonetheless, it appears that salt fingers are stronger on the left side of Figure 8 and differential diffusion tends to be stronger on the right side of Figure 8, presumably with a boundary of equal mixing between them. Additionally, as turbulence increases within the differential diffusion region (with a small Ri_T and a large $\varepsilon_a/\nu N^2$), mixing becomes more equal because of the strong turbulence that overpowers the differential diffusion during and/or after mixing. However, this does not seem to be the case in the salt

fingers region, as the higher turbulence actually allows the salt fingers to grow faster during and/or after mixing (approximate regions shown in Figure 16).

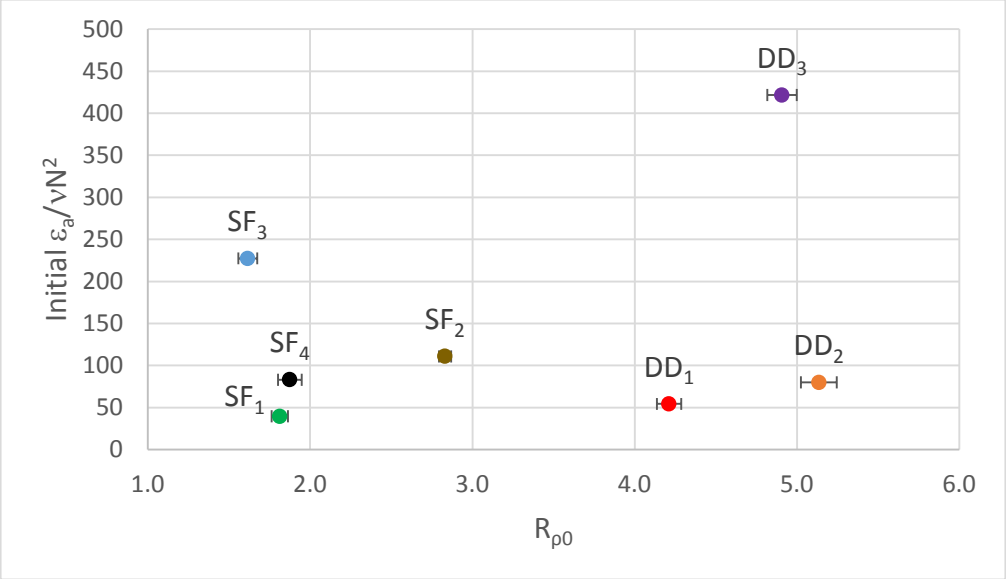

Figure 15. Initial $\varepsilon_a/\nu N^2$ vs. initial R_ρ.

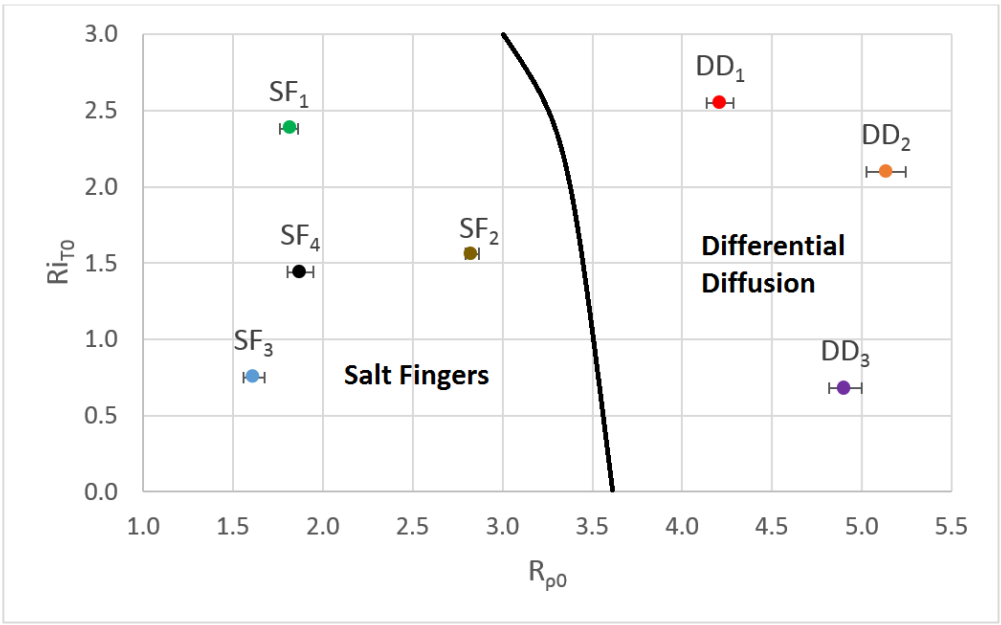

Figure 16. Possible regions of dominant fluxes. Turbulent Richardson number is plotted against density ratio for the initial profile in each experiment.

4.4 Mixing Efficiency

The mixing efficiency was plotted against normalized time for all seven experiments (Figure 17). Examination of the density profiles showed that some of the experiments had more spikes in their initial profile than in the subsequent profiles, likely due to the fact that salt fingers may have been active during filling. Because the initial profile of each experiment significantly affects the mixing efficiency calculations for the remainder of the experiment, mixing efficiency was also calculated using a more stable "initial" profile. Hence, additional mixing efficiencies were calculated and plotted by using the second profile as the "initial" profile and its related N as N_0 for each experiment (Figure 18).

Upon comparison of the mixing efficiency curves, it is evident that mixing efficiency is dependent on both the turbulence and the stratification. It would be expected that mixing efficiencies would be higher for weak turbulence (large Ri_T and small $\varepsilon_a/\nu N^2$) than for strong turbulence, as differential diffusion would be stronger and cause the potential energy of the fluid to increase. Additionally, it would be expected that mixing efficiencies would be higher for large values of R_ρ than for small values, as differential diffusion tends to dominate salt fingers when R_ρ is larger.

As expected, experiments DD_2 and DD_1 had the largest differential diffusion, as they have high mixing efficiencies in Figure 17 and the highest mixing efficiencies in Figure 18. Experiment DD_3 had a similar R_ρ to experiments DD_2 and DD_1, but it had stronger turbulence, so it has a lower mixing efficiency. Although experiments SF_1 and SF_3 have similar R_ρ, experiment SF_1 would be expected to have a higher mixing efficiency than experiment SF_3, as it experiences less turbulence. Their mixing efficiencies are approximately equal in Figure 18, although experiment SF_1 begins with a slight negative mixing efficiency in Figure 18; however,

experiment SF_1 has a higher mixing efficiency in Figure 17 as expected. Additionally, experiment SF_4 would be expected to have a lower mixing efficiency than experiment SF_1 and a higher mixing efficiency than experiment SF_3. In Figure 17, experiment SF_4 has a lower mixing efficiency than both of them and in Figure 18 it has a higher mixing efficiency than both of them. Finally, experiment SF_2 would be expected to have a higher mixing efficiency than experiment SF_4, as it has a larger R_ρ. Experiment SF_2 and SF_4 have about the same mixing efficiency in Figure 18, but SF_2 has a smaller mixing efficiency in Figure 17.

The results of experiments SF_2 and SF_4 are interesting, as they initially have negative mixing efficiencies in Figure 17. Experiment SF_1 also begins with a negative mixing efficiency in Figure 18, but it has a positive mixing efficiency for all subsequent points. Negative mixing efficiencies are possible if E_b decreases during a mixing period, which would occur if the densities profiles were affected more by the salt on the top moving downwards than by the cold water at the bottom moving upwards. That may be what occurs towards the beginning of the experiments, until differential diffusion fluxes increase and the mixing efficiencies become positive. Overall, although the mixing efficiencies do not always behave exactly as expected, generally they show that mixing is more efficient in regions where differential diffusion fluxes are stronger, with weak turbulence (large Ri_T and small $\varepsilon_a/\nu N^2$) and a large R_ρ, than for conditions more conducive to salt fingers.

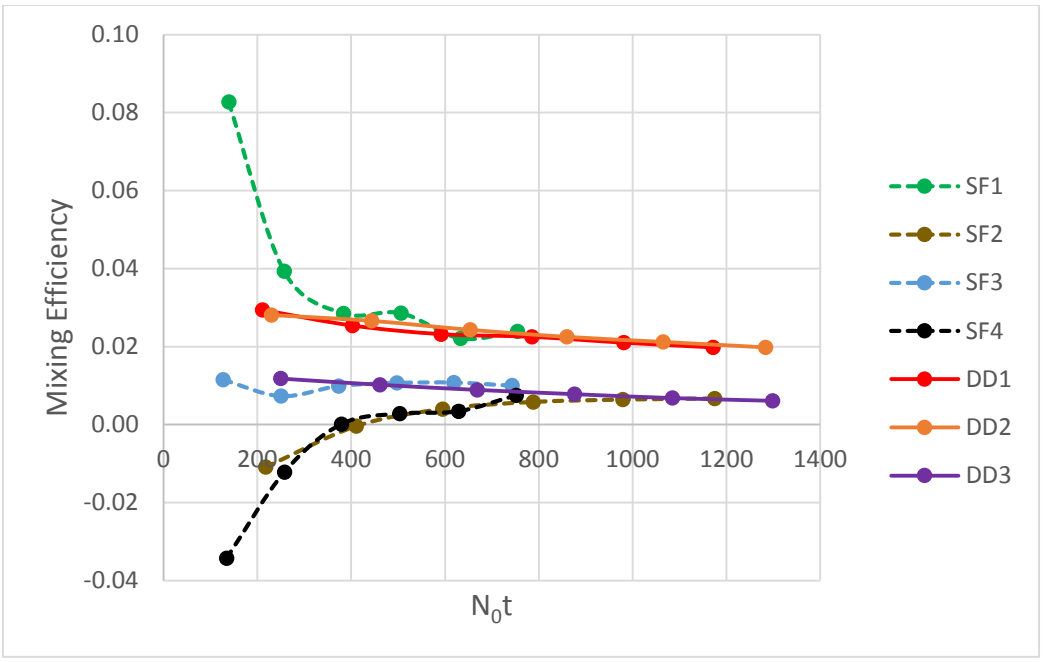

Figure 17. Mixing efficiency vs. N_0t.

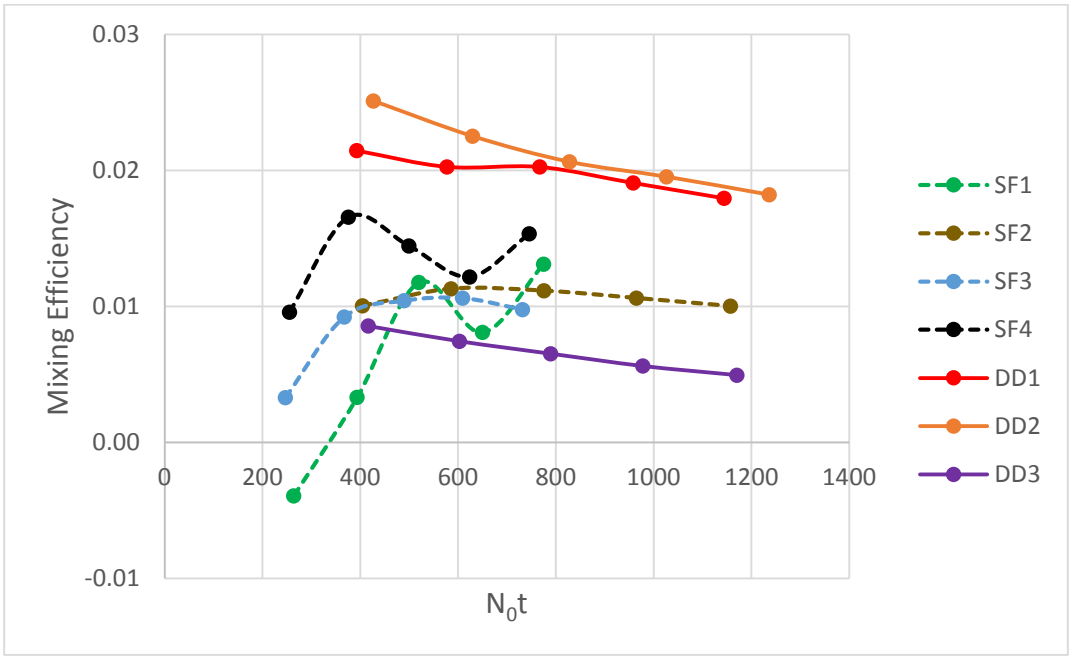

Figure 18. Alternative mixing efficiency vs. N_0t. Mixing efficiency is calculated by using the second profile of each experiment as the "initial" profile and the N from the second profile as N_0.

CHAPTER 5. CONCLUSION

In this study, a series of laboratory experiments was run with a range of stable temperature profiles, unstable salinity profiles, and stable density profiles. Mixing periods were run at a selected level of turbulent mixing intensity for each experiment, and the fluid was profiled after each mixing period to determine how the profiles had changed. Overall, the results showed that salt fingers and differential diffusion were both present during stable-unstable conditions with turbulence, corroborating the first hypothesis. When R_ρ was between 1 and approximately 3, salt finger fluxes were dominant and caused the salinity to mix faster than the temperature. When R_ρ was greater than about 4, differential diffusion fluxes appeared to be dominant and caused temperature to mix faster than salinity. Somewhere in between these values, there is likely a boundary where differential diffusion and salt finger fluxes would be approximately equal. This is consistent with the work of Merryfield (1999) and others, who found that salt fingers are typically strongest when R_ρ is just above 1.

The differential diffusion and salt finger fluxes were also dependent on the turbulence in the fluid. As expected in the second hypothesis, differential diffusion fluxes were stronger for large Ri_T than for small Ri_T. However, surprisingly salt finger fluxes were stronger for small Ri_T than for large Ri_T. This suggests that salt fingers were either active during mixing or grew more rapidly than expected during the time between mixing periods (values varied between 172 and 305 seconds), both of which do not align with the work of Taylor (1991). This could be because during strong turbulence differential diffusion fluxes would be weak, so if there were any salt finger fluxes, R_ρ could start to rise. Between mixing periods salt fingers would continue to grow, presumably leading to a large increase in R_ρ by the time profiles were taken. During weak turbulence differential diffusion fluxes would be stronger, so they would counteract any

preferential transport of salt by salt finger fluxes, making R_ρ decrease or remain basically constant. Between mixing periods salt fingers would grow, presumably leading to a moderate increase in R_ρ by the time profiles were taken.

During periods of turbulence, the mixing efficiencies were generally highest in the regions that were most conducive to differential diffusion, as expected in the third hypothesis. Areas of weak turbulence (large Ri_T and small $\varepsilon_a/\nu N^2$) tend to be preferential to differential diffusion, and differential diffusion also tends to be dominant when R_ρ is larger, causing the mixing efficiencies to increase. This aligns with the work of Jackson and Rehmann (2003), who found that mixing efficiency, as they defined it, tended to be higher for larger values of Ri_T and R_ρ. Differential diffusion will be stronger for weaker turbulence, but even during and/or between periods of strong intermittent turbulence salt fingers can grow rapidly.

Although care must be taken in applying laboratory results to the ocean, this study shows that salt fingers and differential diffusion can both be present during stable-unstable conditions, which occur in the subtropical oceans. Whether salt fingers and/or differential diffusion fluxes are active depends on the stratification and turbulence of the fluid. When conditions are more conducive to differential diffusion, the mixing efficiency of the fluid will also tend to be higher. If ocean models allowed for the fact that temperature and salinity mix at different rates depending on the diffusive fluxes active, they could be used to more accurately predict climate conditions.

REFERENCES

Broadwell, J. E., and M. G. Mungal, 1991: Large-scale structures and molecular mixing. *Phys. Fluids A,* **3,** 1193–1206.

Bryan, F., 1987: Parameter Sensitivity of Primitive Equation Ocean General Circulation Models. *J. Phys. Oceanogr.,* **17,** 970–985.

Gargett, A. E., 1984: Vertical eddy diffusivity in the ocean interior. *J. Mar. Res.,* **46,** 359–393.

— —, 1986: Small-scale parameterization in large-scale ocean models. In *Advanced Physical Oceanographic Numerical Modelling*, ed. J. J. O'Brien. Reidel Publishing Co., 145–154.

— —, and B. Ferron, 1996: The effects of differential vertical diffusion of *T* and *S* in a box model of thermohaline circulation. *J. Mar. Res.,* **54,** 827–866.

IPCC (Intergovernmental Panel on Climate Change), 1990: Houghton, J. T., G. J. Jenkins and J. J. Ephraums, eds. Climate Change: The IPCC Scientific Assessment. *Cambridge Univ. Press,* 364 pp.

Jackson, P. R., 2001: Effects of differential diffusion on mixing efficiency in a diffusively-stable, turbulent flow. M.S. thesis, University of Illinois.

— —, and C. R. Rehmann, 2003: Laboratory measurements of differential diffusion in a diffusively stable, turbulent flow. *J. Phys. Oceanogr.,* **33,** 1592–1603.

Kunze, E., 1987: Limits on growing, finite-length salt fingers: A Richardson number constraint. *J. Mar. Res.,* **45,** 533–556.

Linden, P. F., 1971: Salt fingers in the presence of grid-generated turbulence. *J. Fluid Mech.,* **49,** 611–624.

Martin, J. E., and C. R. Rehmann, 2006: Layering in a flow with diffusively stable temperature and salinity stratification. *J. Phys. Oceanogr.,* **36**, 1457–1470.

McDougall, T. J., and J. R. Taylor, 1984: Flux measurements across a finger interface at low values of the stability ratio. *J. Mar. Res.,* **42,** 1–14.

— —, and B. R. Ruddick, 1992: The use of ocean microstructure quantify both turbulent mixing and salt fingering. *Deep-Sea Research,* **39,** 1931–1952.

Merryfield, W. J., G. Holloway, and A. E. Gargett, 1998: Differential vertical transport of heat and salt by weak stratified turbulence. *Geophys. Res. Letters,* **25,** 2773–2776.

— —, — —, and — —, 1999: A global ocean model with double diffusive mixing. *J. Phys. Oceanogr.,* **29,** 1124–1142.

— —, 2002: Intrusions in doubly-stable Arctic waters: evidence for differential mixing? *J. Phys. Oceanogr.,* **32,** 1452–1451.

Morrison, F.A., 2014: Obtaining uncertainty measures on slope and intercept of a least squares fit with Excel's LINEST. *Unpublished manuscript,* Michigan Technological University, Houghton, MI.

Nash, J. D., and J. N. Moum, 2002: Microstructure estimates of turbulent salinity flux and the dissipation spectrum of salinity. *J. Phys. Oceanogr.,* **32,** 2312–2333.

Rehmann, C. R., 1995: Effects of stratification and molecular diffusivity on the mixing efficiency of decaying grid turbulence. Ph.D. thesis, Stanford University.

— —, and J. R. Koseff, 2004: Mean potential energy change in stratified grid turbulence. *Dyn. Atmos. Oceans,* **37**, 271–294.

Schmitt, R. W., and D. L. Evans, 1978: An estimate of the vertical mixing due to salt fingers based on observations in the North Atlantic Central Water, *J. Geophys. Res.,* **83,** 2913–2919.

— —, 1979: The growth rate of super-critical salt fingers. *Deep-Sea Research,* **26A,** 23–40.

— —, 1981: Form of the temperature-salinity relationship in the Central Water: evidence for double-diffusive mixing. *Journal of Physical Oceanography*, ***11,*** 1015–1026

— —, 1988: Mixing in a thermohaline staircase. *Small-Scale Turbulence and Mixing in the Ocean,* J. C. J. Nihoul and B. M. Jamart, Eds., Elsevier, 435–452.

— —, 2003: Observational and laboratory insights into salt finger convection. *Progress in Oceanography,* **56,** 419–433.

Smyth, W. D., J. D. Nash, and J. N. Moum, 2005: Differential diffusion in Breaking Kelvin–Helmholtz Billows. *J. Phys. Oceanogr.*, **35**, 1004–1022.

Taylor, J., 1991: Laboratory experiments on the formation of salt fingers after the decay of turbulence. *Journal of Geophysical Research*, ***96,*** 12497–12510.

Walsh, D., and B. Ruddick 1995: An investigation of Kunze's salt finger flux laws-Are they stable?. In *Double-Diffusive Convection,* eds. A. Brandt and H. J. S. Fernando. American Geophysical Union, Washington, D. C., **94,** 321– 328.

Wells, M. G., and R. W. Griffiths, 2003: Interaction of salt finger convection with intermittent turbulence. *J. Geophys. Res.*, **108,** 3080, doi:10.1029/2002JC001427, C3.

Wykes, M. S. D., and S. B. Dalziel, 2014: Efficient mixing in stratified flows: Experimental study of a Rayleigh-Taylor unstable interface with an otherwise stable stratification. *J. Fluid Mech.* **756**, 1027–1057.

Zhang, J., R. W. Schmitt, and R. X. Huang, 1998: Sensitivity of GFDL Modular Ocean Model to the parameterization of double-diffusive processes. *J. Phys. Oceanogr.*, **28,** 589–605.